Tungsten (2021) 3:20–37
https://doi.org/10.1007/s42864-021-00075-9

Tungsten
www.springer.com/42864

REVIEW PAPER

Recent progress of radiation response in nanostructured tungsten for nuclear application

Hang Xu[1] · Lan-Li He[1] · Yong-Feng Pei[1] · Chang-Zhong Jiang[1] · Wen-Qing Li[1] · Xiang-Heng Xiao[1]

Received: 2 October 2020 / Revised: 29 October 2020 / Accepted: 30 October 2020 / Published online: 5 March 2021

Abstract
Engineering materials for nuclear reactors exposed to high-dose irradiation breed various radiation damage, leading to performance degradation of materials, which seriously limits the application of materials in the future advanced nuclear reactors. Tungsten-based materials applied in future nuclear reactors have to withstand not only the attack of high-energy neutron and plasma, but also the repeated impact of steady-state or even transient thermal load. Researches in the past decades have proved that tailored nanostructure have advantage in annihilating radiation defects. With the rapid development of nanostructured tungsten, probing radiation application of nanostructured tungsten is of great significance in promoting the development of novel radiation-resistant materials. Herein, the development status of three kinds of nanostructured tungsten namely nanocrystalline, nanofilm and nanoporous tungsten designed for radiation tolerance and the performance enhancement mechanism of diverse nanostructure in irradiation environment is reviewed. Finally, future perspectives and technical challenges are discussed, to inspire more creative designs of novel nanostructured tungsten for radiation tolerance.

Keywords Tungsten · Nanostructure · Radiation damage · Radiation resistance

1 Introduction

The safe and stable conduction of the nuclear reactor is inseparable from the resistance of nuclear-grade engineering materials under harsh irradiation. As a refractory transition metal with extremely high melting point, tungsten has been considered to be primary candidate for the plasma facing materials (PFMs) in the future fusion reactor [1]. Recently, many efforts have been done to fabricate tungsten-based materials with desired properties for advanced fission and fusion application by doping alloy elements [2–6] or dispersoid strengthening [7–10]. Tungsten-based PFMs will be directly exposed to 10–10^4 MeV plasma and 14.1 MeV neutron radiation in the fusion reactor [11–13]. During radiation the mechanical and thermal properties of tungsten are impacted by particle irradiation, due to cascade collision caused by neutron and nuclear transmutation atoms. Further radiation defects such as blister [14–16] and nanotendrils [17–19] tend to form in tungsten-based materials by the accumulation of primary point defects, eventually resulting in irreversible degradation of performance, such as irradiation hardening, amorphization, and improvement of the ductile-to-brittle transition temperature [20–22].

Nanostructures have been deliberately designed to improve the radiation resistance of nuclear engineering materials. It has been verified that grain boundaries, phase boundaries, and free surfaces in nanostructured materials act as defect traps or release sites, accelerating the evolution and self-healing of defects [23–28]. The design of radiation-resistant nanostructured materials has inspired nanostructuring of tungsten-based materials which are expected to own remarkable radiation tolerance in harsh environment. This paper presents the current status of novel tungsten-based nanostructured material for radiation resistance application. The performance of nanostructured tungsten in radiation experiments are discussed in detail, as well as the simulation calculation of enhancement mechanism. At the end of each chapter, the technical challenges and prospects of different tungsten-based nanostructures are mentioned.

✉ Wen-Qing Li
wenqing_li@whu.edu.cn

✉ Xiang-Heng Xiao
xxh@whu.edu.cn

[1] Hubei Nuclear Solid Physics Key Laboratory, Department of Physics, Wuhan University, Wuhan 430072, China

2 Nanocrystalline tungsten for radiation resistance

Various nanocrystalline materials have been developed for radiation resistance [29–31]. In coarse-grain material, the diffusion barrier of vacancies is high, and hence the irradiation-induced vacancies migrate slowly and hard to recombine with interstitial atoms. These vacancies are accumulated in the matrix, resulting in irradiation embrittlement [32]. Generally, nanocrystalline materials contain abundant grain boundaries (GBs) and phase boundaries of dispersed particles, and these interfaces act as annihilation sites for interstitial atoms and vacancies [33], and thereby the radiation effect of nanocrystalline significantly differs from coarse grain.

The first-wall materials developed for fusion application would face hundreds of dpa (displacement per atom) neutron irradiation during the expected 3–5 years lifetime [34]. The conventional coarse-grained tungsten (CGW) will be seriously degraded under such harsh environment. Compared with CGW, the nanocrystalline tungsten (NCW) is expected to have superior tolerance to harsh irradiation and high temperature. Besides, nanocrystallization is the most convenient way to obtain nanostructured tungsten.

2.1 Preparation of nanocrystalline tungsten

The preparation of nanocrystalline tungsten is critical due to refractory and hardness of tungsten. In the process of preparation, the formation of small and dense nanocrystalline tungsten is inseparable with refinement mode and work temperature. Several effective processes for obtaining tungsten-based nanocrystalline are introduced below.

Powder metallurgy is the common route to prepare nanocrystalline tungsten. In this route, the most critical step is powder densification. Nanocrystalline is constructed by nano or micron tungsten powders forming metallurgical bonds during densification. So far, the W bulk densification techniques include pressureless sintering (PLS) and pressure sintering that is subdivided into spark plasma sintering (SPS), ultrahigh pressure (UHP), hot isostatic pressing (HIP), and hot pressing (HP). PLS is a traditional sintering method, which is often applied in mass production of tungsten. However, it is hard to obtain fine grains and high density of W bulk materials by this way due to the inevitable grain coarsening during the sintering. The intervention of pressure is necessary in the preparation of nanocrystalline tungsten. Recently, the W–5 wt% Ta alloy with average size of 1.73 μm was prepared via the SPS technology. Wu et al. [35] proposed 10 nm W–5 wt% Y_2O_3 (WYO) and 85 nm W–5 wt% Y_2O_3–2.5 wt% Ni (WYON) designed for radiation resistance, and these tungsten-based alloys were fabricated by resistance sintering under ultrahigh pressure (RSUHP).

Another method to reduce tungsten grain size to nanoscale is severe plastic deformation (SPD) [36–38]. The initial SPD effectively decreases grain size and brittleness, but NCW obtained in this way tends to grow and coarsen at elevated temperatures. With the innovation of severe deformation technology, stable ultra-fine, and nano-grain tungsten have been fabricated by equal channel angular extrusion (ECAP) and high-pressure torsion (HTP) [39–41]. And nanocrystalline pure tungsten introduced in the next chapter is mostly prepared by this method.

2.2 Radiation damage in pure nanocrystalline tungsten

Nanocrystalline boundaries have been proved as effective sinks to absorb the point defects, resulting in mitigation of irradiation-induced dislocation loops and void swelling. There are two typical modes of GBs absorption defects in nanocrystalline. In detail, the absorption process of nanocrystalline Ni in Kr ion radiation by in situ transmission electron microscope (TEM) is revealed by Sun et al. [42]. First, the dislocation loop shrank slowly and was swiftly absorbed by nearby high-angle grain boundary (HAGB). In another condition, GBs were considered to gradually absorb the dislocation segment consisting of dislocation loops in about twice the time. The activation energy of dislocation loop diffusion near GBs decreases, which made loops easier to move than in the bulk region. Meanwhile, due to the existence of vacancy concentration gradient, these dislocation loops preferentially diffuse to boundaries. Atomic-scale simulations [43] have shown GBs emit interstitial atoms to combine with the nearby vacancies improving vacancy migration at boundaries loaded with interstitials, and the defect annihilations greatly depend on the local boundary structure and have been simulated in Cu and Fe [44, 45].

The nanocrystalline tungsten was manufactured with grain sizes from submicron to nanoscale by severe surface deformation [46]. As shown in Fig. 1a–d, in situ TEM observation showed that numerous point defect clusters existed in ultra-fine grains (marked as 2 and 3) while nanocrystalline (marked as 1) demonstrates a uniform distribution of bubbles and significantly lower density of defect clusters. And in NCW, more bubbles were observed decorating in the nano-grain boundaries rather than intra-grain as indicated in Fig. 1e–h, which was the strong evidence that the nanocrystalline tungsten boundaries effectively capture interstitial He atoms. A special dislocation loop "raft" structure formed by dislocation loop glide and cluster interaction in tungsten has been reported under neutron and heavy ion irradiation [47, 48]. But no raft was observed at RT in the nanocrystalline

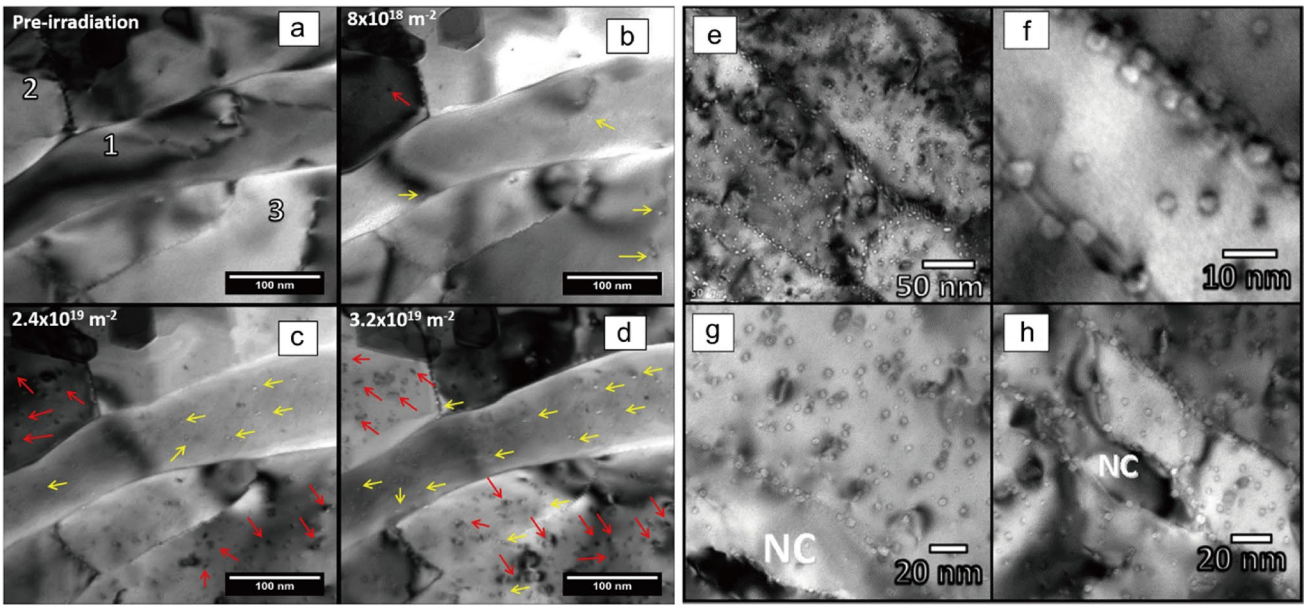

Fig. 1 **a–d** In situ TEM observation of nanocrystalline and ultra-fine grain in 2-keV He ion irradiation experiment at 1123 K. **a** Pre-irradiated nanocrystalline. **b** After 8×10^{14} ions·cm^{-2} He ion radiation. Bubbles are indicated by yellow arrows. **c** After 2.4×10^{15} ions·cm^{-2} He ion radiation. Point defect clusters indicated by red arrows are found in ultra-fine grain. **d** After 3.2×10^{15} ions·cm^{-2} He ion radiation. **e–h** Ultra-fine grain and nanocrystalline in 2-keV He ion irradiation experiment with a fluence of 3.6×10^{15} ions·cm^{-2} at 1123 K. **e** Low magnification and **f** high magnification micrograph image exhibiting He bubbles distributed around GBs, and **g, h** evident lower densities of bubbles observed compared to ultra-fine grains. Reproduced with permission from Ref. [46]. Copyright 2014 Springer Nature

grains at about 0.25 dpa, which was attributed to efficient absorption of interstitials by the GBs. Further research [49] focused on radiation response of CGW and bimodal W (containing nanocrystalline and ultra-fine grain) radiated by 3 MeV Cu ion at different irradiation rates and temperatures. After Cu radiation up to 4 dpa, all samples possessed similar damage types, but 50–600 nm bimodal W showed less void swelling at all dose radiation compared to CGW. The formation of voids without denudation at 1050 K indicates that the growth of voids comes from local vacancy loop sites, which are attributed to vacancy absorption at high temperature. El-Atwani et al. [50] reported that nanocrystalline boundaries in equiaxed tungsten can absorb dislocation loops rapidly and continuously as shown in Fig. 2a, and this absorption is enhanced at high temperature. Figure 2b shows the statistical result of void density, average void size, and swelling condition of three types with different grain size at 2 dpa. The void density in nanocrystalline W–85 nm is highest since the less annihilation of small void nucleation due to less interstitials and interstitial loops existence. On the contrary, the void size and change of volume of 85 nm grain are least in these observations, which indicated that NCW possess the resistance to swelling. It is interesting that radiation-induced defects aggregate in stressed grains as shown in Fig. 2c, which indicated stress fields around grain boundary might affect defect absorption.

The solubility of He in tungsten is very low, and thereby the He radiation-induced damage might cause the fluctuation of the stress state and even crack in nanocrystalline tungsten. To probe the crack formation mechanisms of NCW in He ion irradiation, Chen et al. [51] compared different blister behavior of NCW and CGW in detail through the helium ion microscope. In the nanocrystalline, only crack formation was found along GBs even at the dose of 5×10^{17} ion·cm^{-2}, while obvious bubbles and continuous crack occurred at a low dose in CGW. As shown in Fig. 3a, b, at the same dose, the blister induced crack size in nanocrystals is much smaller than that in CGW. Figure 3c, d demonstrated the simulated process of microstructure evolution under diverse tensile strain levels, and the result showed that the morphology and propagation behavior of cracks in nanocrystalline were greatly affected by He clusters, as He atoms could readily cluster and coalesce via trap evolution and loop punching mechanisms. Noteworthy, the HAGB seems to be more effective in hindering crack propagation compared to their low-angle counterparts. In the case of typical low-angle grain boundaries (LAGBs) as shown in Fig. 3c, several cracks were initiated by the growth of He clusters through loop punching, subsequently, these cracks coalesced, resulting in a rapid crack growth.

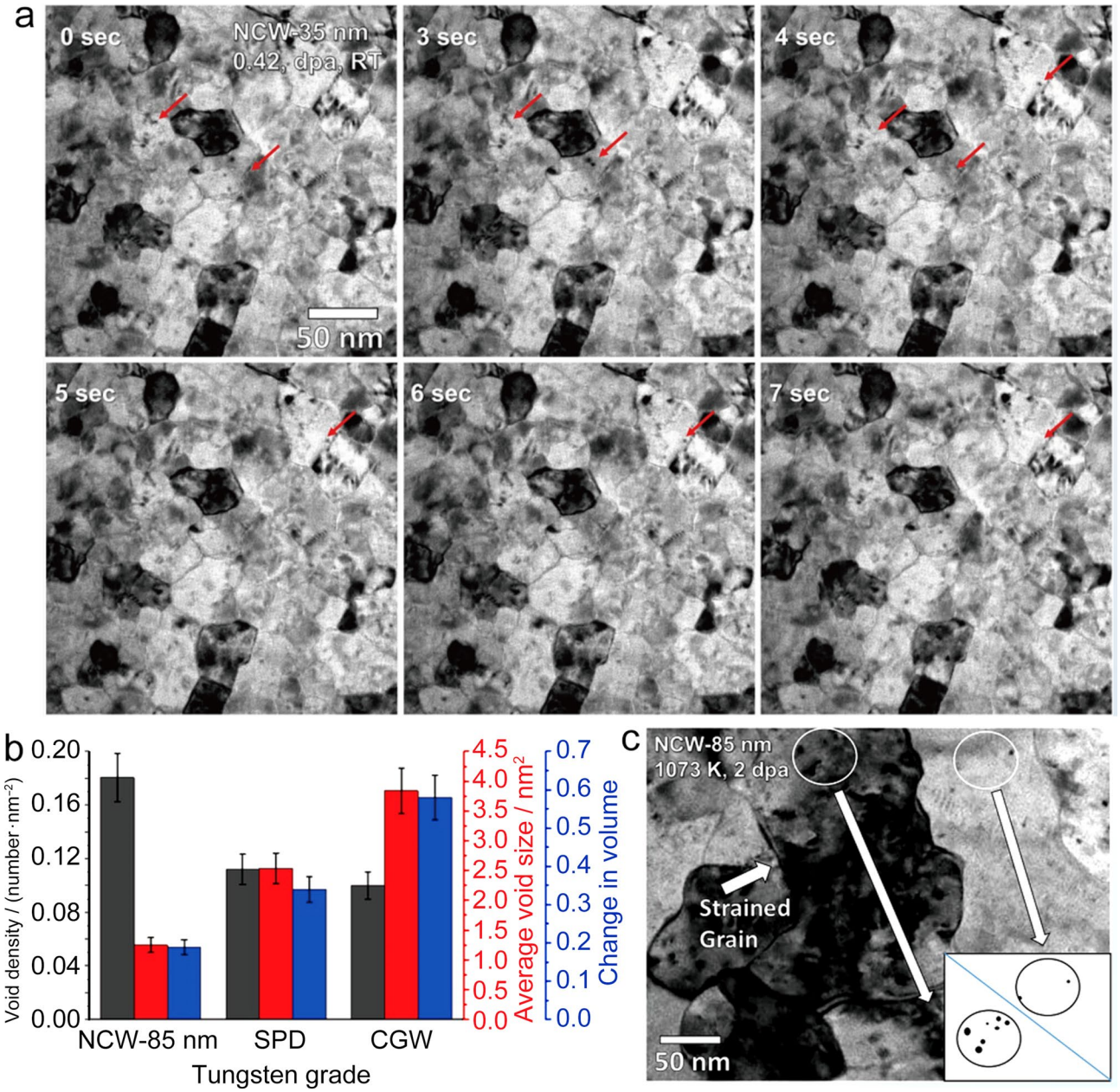

Fig. 2 **a** Snapshots TEM micrographs of nanocrystalline W–35 nm during 1-MeV Kr ion irradiation of around 0.42 dpa at room temperature; **b** void density, average void size and the swelling condition in tungsten with various sizes after radiation at 1073 K; **c** TEM image of irradiated 85-nm nanocrystalline W at 1073 K. In the higher strain (dark grain) region more and larger defects are found, and the inset illustrate these defect distributions. Reproduced with permission from Ref. [50]. Copyright 2019 Elsevier

2.3 Radiation response of alloying nanocrystalline tungsten

Alloying is often used in the construction of NCW to reinforce strength and radiation resistance. According to the first-principles calculation [52], the transition metal elements with larger electronegativity tend to bond to vacancies and smaller elements prefer to bond to self-interstitials in tungsten, and thus alloy elements will significantly affect the radiation resistance of the tungsten matrix. In addition, excessive alloy elements precipitating in the form of the second-phase particle can compensate for the degeneration of thermal stability in nanocrystalline [53]. Oxides and carbides are common precipitates in nanocrystalline tungsten. Kurishita et al. [54–56] fabricated 50–190 nm W–TiC alloys by hot isostatic pressing (HIP) with bend fracture strength of about 2 GPa. After 3 MeV He radiation, critical fluence for surface cracking in ultra-fine grained W–TiC is over 10

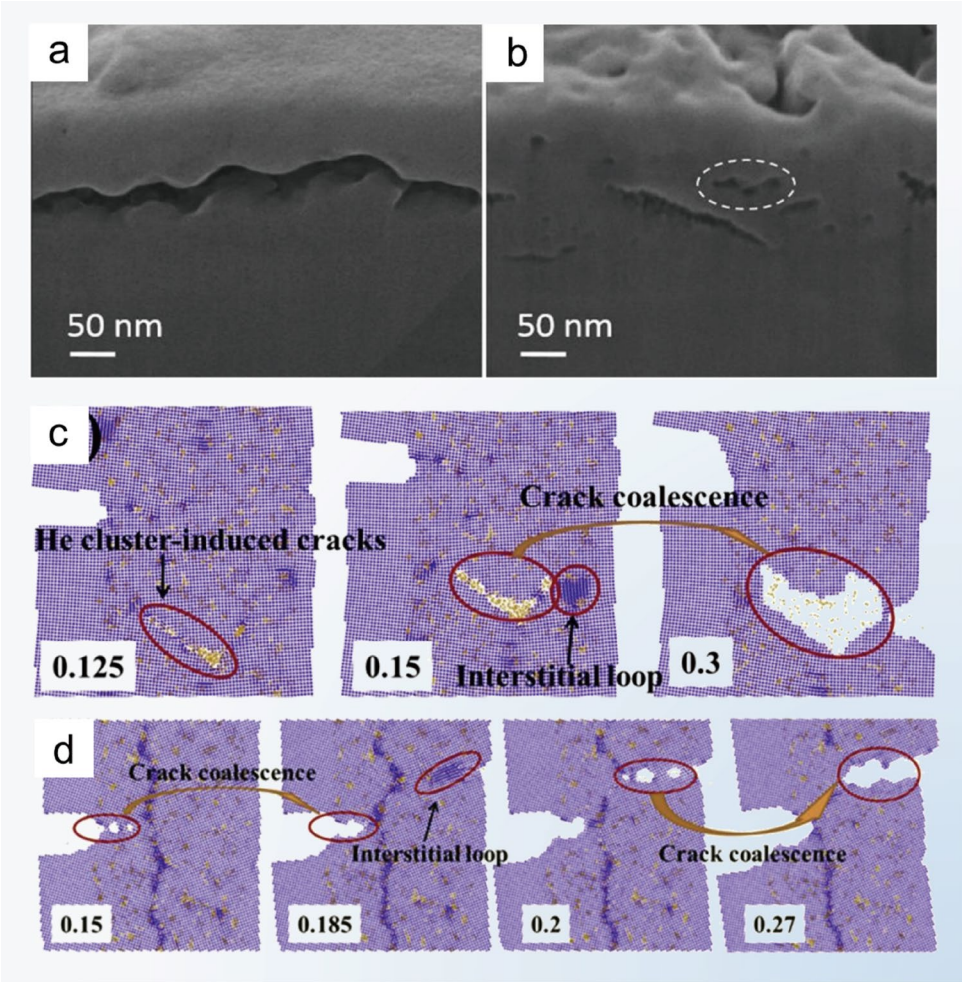

Fig. 3 Cross-sectional images of the blister and crack microstructure of **a** CGW and **b** nanocrystalline W after He irradiation with a fluence of 1×10^{19} ions·cm^{-2}, respectively; simulated microstructural evolution of GB with 10% He at dynamic strain levels under the tensile loading related to **c** LAGB bicrystal and **d** HAGB. The blue and orange color represent tungsten and helium atoms, respectively. Reproduced with permission from Ref. [51]. Copyright 2018 Elsevier

times than that in commercial W. Another study [57] involving ultra-fine W–TiC showed that W–TiC alloy had better radiation tolerance and less total loop and void damage than those of CGW at 1073 K during in situ Kr irradiation observation. Although there was no obvious difference in loop density, the average loop area in W–TiC was much smaller and decreased with time. The effect of dispersoid TiC is emphasized, which might be the cause of the increase in total loop damage at high temperatures. Fukuda et al. [58] reported the effect of neutron irradiation on performances of ultrafine-grained (UFG) W–TiC alloys and other coarse W alloys in the experimental fast reactor. It was confirmed that the UFG W–TiC of which part is nanocrystalline had a low rate of hardening after up to 0.42 dpa neutron irradiation at 1049 K, and NCW exhibited a much smaller number density of neutron irradiation-induced voids than that of pure W [59]. Wu et al. [35] discussed the irradiation tolerance of 10 nm WYO and 85 nm WYON. The WYO with average grain size of 10 nm had significantly low swelling rate and bubble density at all He irradiation doses, although the bubble size fluctuated slightly. Recently, a quaternary W-based high-entropy alloy (HEA) W–Ta–V–Cr were manufactured [60], and the HEA film exhibited bimodal grain size distribution in the nano and submicron scale. Although only around 70% grains belong to nanocrystalline, no evident irradiation-induced damage was found in situ. Remarkably, the second-phase particles are rich in Cr and V precipitation in the form of spheres after irradiation. And a rate theoretical model has been constructed to probe the origin of precipitates, proving Cr and V own a strong segregation tendency, which is consistent with experimental results. The fact that these alloys with outstanding radiation resistance are potential for bulk production makes them ideal structural materials for applications requiring extreme irradiation conditions.

2.4 Challenges of nanocrystalline tungsten

The meticulous design of nanocrystalline not only enhances the mechanical properties, but also provides great potential in improving the resistance of materials to harsh irradiation. Before wide utilization of nanocrystalline tungsten, several problems need to be further explored.

Firstly, in several studies at present it is seemly hard to obtain uniform nanocrystalline tungsten via conventional preparation, the growth of nano-grain at elevated temperature inevitably results in the bimodal grain size distribution in current nanocrystalline. Therefore, the further innovation of forming process and continuous deformation are necessary to obtain finer and uniform tungsten grains. Recently, several ultra-uniform nanocrystalline materials were reported via a two-step sintering, which is expected to be used in the tungsten-based nanocrystalline [61, 62]. Furthermore, doping elements precipitating around the boundary in the form of oxide nano-clusters could effectively stabilize nano-grain in austenite steel, and this strategy may also encourage the construction of stable tungsten-based nanocrystalline at elevated temperature [31].

However, though the accumulation of radiation defects at GBs has notable benefits in the irradiation performance of nanocrystalline, GBs with aggregated defects may degrade the mechanical properties with the dose increasing. Characteristics of GBs transform with the absorption of point defects, which would be a hidden hazard for nanocrystalline tungsten under the higher dose irradiation for long time.

Other vital issues, such as transmutation-induced precipitation [63] and thermal stability [64] of tungsten-based materials under high-dose irradiation, have been studied in micrometer-scale, but relevant research is not abundant to reveal the microscopic and atomic behavior mechanism of irradiated nanocrystalline tungsten.

3 Radiation-tolerant nanofilm tungsten

Nanofilm material is one kind of nanocomposite formed on the substrate, which is composed of discontinuous layers alternately stacking including metals and non-metal layers with nanoscale thickness. Multilayered nanofilm exhibiting unique properties has been widely studied in various fields, such as superhard film [65–67], giant magneto-resistance [68], corrosion-resistance [69], and thermal insulation [70]. The interfaces in multilayer structures can provide sites for trapping defects which are similar to the numerous GBs in nanocrystalline. In the direction of thickness, the coarsening of nanolayers could be inhibited by the existence of interlayer interface in multilayered nanofilms. Tungsten-based nano-multilayers with high melting point ensure the outstanding performance of nanostructure in thermal stability [71, 72]. Nanofilm material with refractory tungsten layer as one of the components decreases the sensitivity to electron energy loss, which is competitive for future nuclear protect application [73]. In recent years, many tungsten-based nano-multilayers which were applied in radiation tolerance have been prepared as shown in Fig. 4 [74–78].

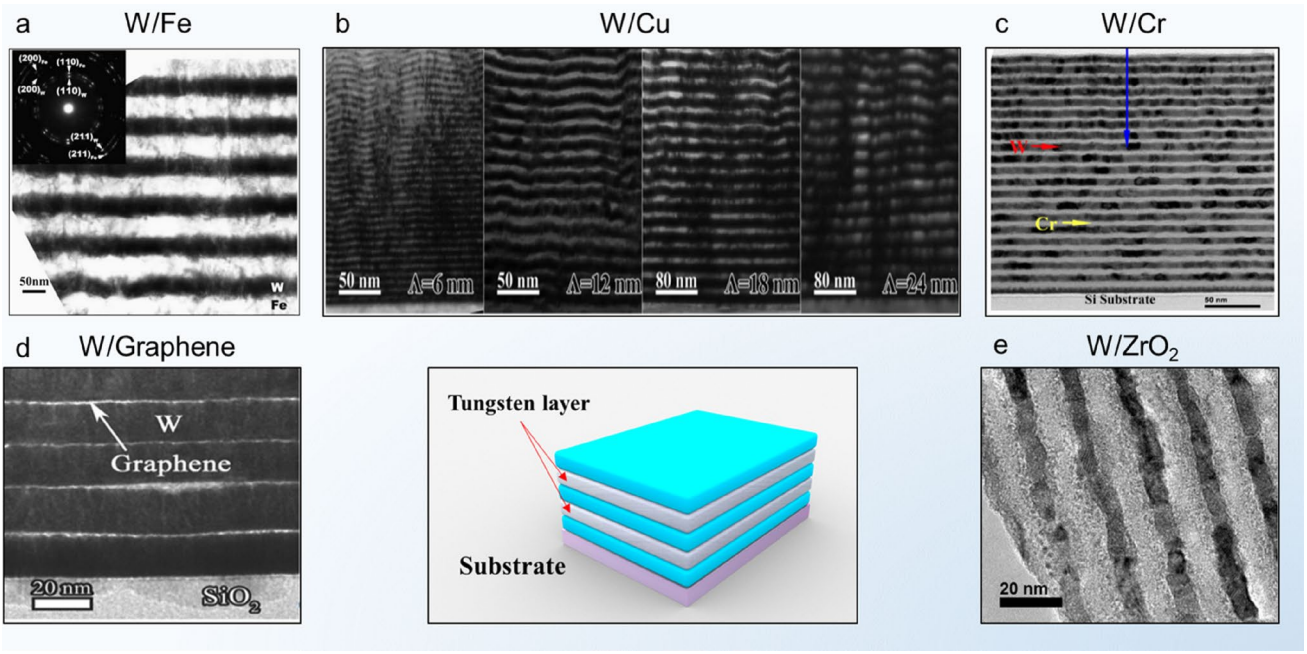

Fig. 4 Micrograph images of various nanofilm tungsten: **a** W/Fe. Reproduced with permission from Ref. [74]. Copyright 2009 Elsevier; **b** W/Cu. Reproduced with permission from Ref. [75]. Copyright 2017 Elsevier; **c** W/Cr. Reproduced with permission from Ref. [76]. Copyright 2015 Elsevier; **d** W/graphene. Reproduced with permission from Ref. [77]. Copyright 2017 Wiley; **e** W/ZrO_2. Reproduced with permission from Ref. [78]. Copyright 2014 Elsevier

3.1 Interface construction of nanofilm structure

Nanofilm structures are metastable and tend to the low-energy status due to the existence of high volume fraction phase interface and grain boundary. For instance, in the Cu/Ni multilayer [79], adjacent atoms aside of the interface spread across the phase boundaries and form a solid solution or compound at elevated temperature, which reduced the composition gradient of the interface, and eventually resulted in the gradual disappearance of the layered structure. On the other hand, if both sides of the interface are completely insoluble such as Cu/Nb [80] and Cu/Ag [81], the atoms would diffuse along with the interlayer interface, leading to GB grooving at the intersection of the GB and the phase boundary. The immiscible systems (such as Cu/V) and few miscible systems (such as Al/Nb) were proved to be stable under He ion irradiation [82], but another study [83] showed that the Nb_3Al phase was formed at the interface in Al/Nb nano-multilayers after He ion irradiation, and the embedded alloy phase may weaken the radiation resistance of nanofilm structure. Overall, whether components are solid-soluble or not, the selection of nano-layer materials is momentous for radiation resistance of nanofilm structure.

Nevertheless, the metallic nano-multilayers are usually designed into the same thickness in each layer to study the influence of nano-multilayers with diverse thickness towards radiation performance. If metallic layers combine with oxides or other non-metallic layers, the thickness of the two components is often different. In common binary multilayer nanofilms, the periodic thickness is defined as the total thickness of each stacking cycle, which has a significant influence on radiation tolerance of nanofilm structure. Misra et al. [84] and Zhang et al. [85] studied microstructure evolution of Cu/Nb nano-multilayers with a period of 2.5 nm under He ion irradiation, and no obvious He bubbles was found after radiation experiment. Cu/Nb nano-multilayers compared with bulk materials can effectively annihilate the radiation defects and inhibit nucleation and growth of bubble at high temperature. Zhang et al. [82] processed several metal nano-multilayers including Cu/V, Cu/Mo, Fe/W, and Al/Nb, followed with He ions radiation until the peak He concentration reached 4–6 at. %. The result showed that suitable interface greatly suppressed defect accumulation and hardening caused by irradiation. It is worth noting that the size effect exists in all studied systems. Namely the lesser the periodic thickness of the nanofilm structure is, the better radiation resistance it possesses. However, with the increase of interface density, the weakening of other properties (such as thermal conductivity) may occur under strong radiation. Thus, the appropriate thickness period is considerable for comprehensive radiation performance in the nanofilm tungsten.

3.2 Radiation response of metallic nanofilm tungsten

In the initial exploration, miscible W/Fe-multilayered nanofilms [74] were fabricated with different periods, and the interface between binary nanofilm W/Fe is incoherent as the lattice parameter of Fe and W difference is over 10%. After He irradiation (6×10^{16} ions·cm^{-2}), large quantities of He bubbles and evident radiation-induced hardening were observed in 5 and 50 nm Fe/W multilayers. Only 1 nm W/Fe specimens showed no obvious hardening, and obvious interface intermixing was found between W and Fe layers. Meanwhile, W/Cr nano-multilayer [76] irradiated by 3 MeV Xe^{20+} ion exhibited few irradiation-induced swelling compared with pure W films although nanofilm structure cannot prevent phase transition of β-W to α-W. The miscible systems mentioned above showed poor chemical stability of interface, which seems to be detrimental in high-energy irradiation environment.

The W/Cu nanofilm is a typical immiscible face centered cubic (FCC)–body centered cubic (BCC)system with a lattice mismatch of 7%. Gao et al. [86] reported that the W/Cu nanofilm system with the period of 5–100 nm. In the W/Cu system, incoherent interfaces between W and Cu were considered to act as sinks for point defects and Frenkel pairs. After He ion irradiation (up to 70 dpa), W/Cu5 (W/Cu sample with a period of 5 nm) was considered to have the best radiation tolerance with no void found in stable morphological interfaces. On the other hand, He bubbles aligned along the interface were observed in thick period W/Cu. The formation of bubbles was mostly found in Cu layers and along columnar GBs [87], which might result from individual He atom that was allowed to migrate through interfaces or surrounding layers [88]. Dong et al. [75] systematically studied the responses of W/Cu multilayered nanofilms irradiated by 40 keV He^+, 6.4 MeV Xr^{23+} and 200 MeV Xr^{14+} ions, which simulated He bubble damage, neutron irradiation and fission fragment damage, respectively. In the 200 MeV Xr^{14+} radiation, almost all the W and Cu layers maintain their original layered structure except W/Cu12. Structure damage only existed in the bottom layers of the W/Cu12, which were smashed into two or three thin layers with fine broken grain and disappeared with the increase of thickness. Figure 5 shows the details of W/Cu nanofilms with different thickness periods irradiated by 6.4 MeV Xe^{23+}, and the layer interfaces of Cu/W6 and Cu/W18 remain sharp after 6.4 MeV Xe^{23+} irradiation at 7.5×10^{14} ions·cm^{-2} and 1.5×10^{15} ions·cm^{-2} fluence. From Fig. 5f, intermixing layers were observed between W and Cu layers with corresponding displacement damage of 20 dpa. Cu and W atoms are knocked into adjacent layers of which lattices are overlapped to form Moire patterns. The author attributed the interaction

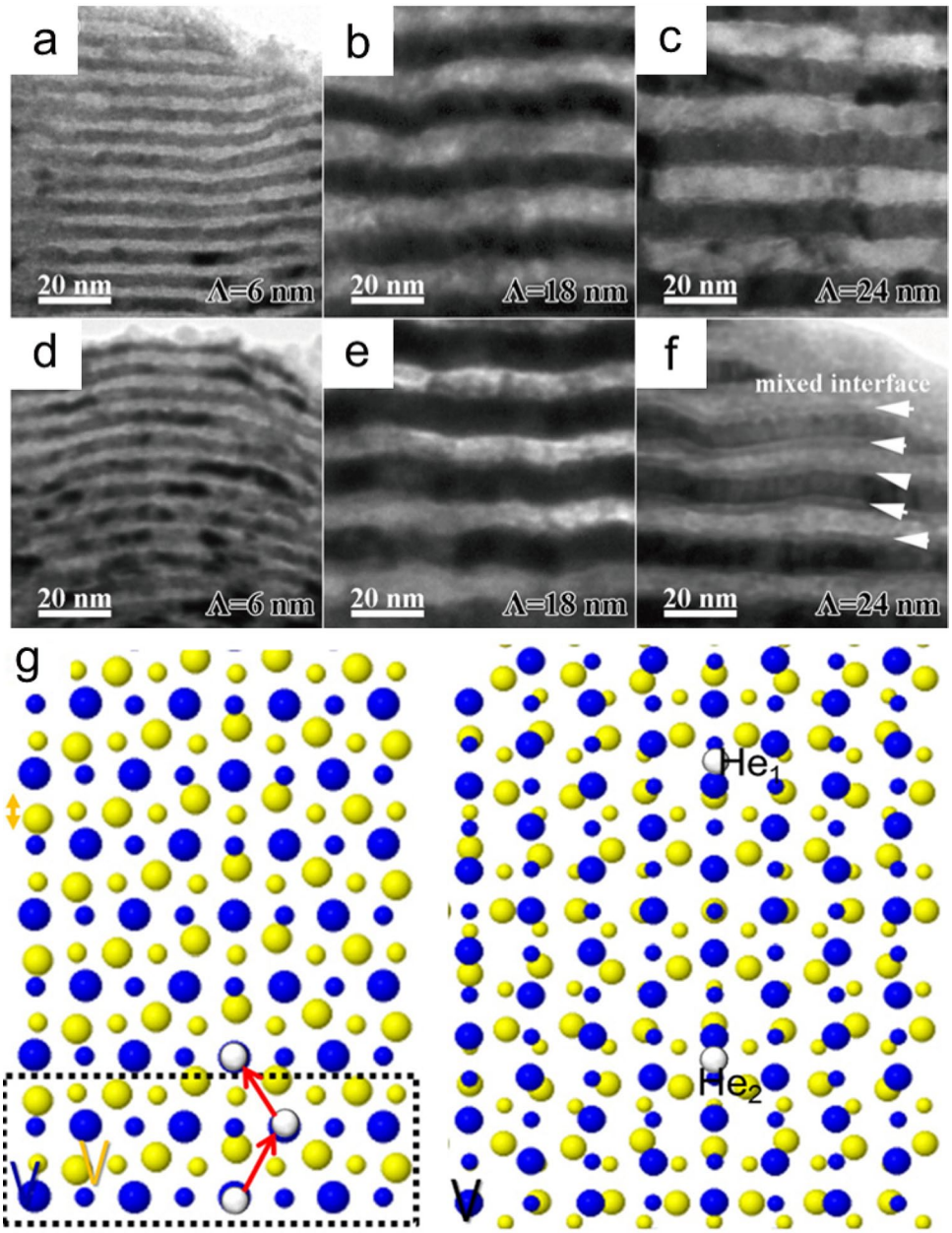

Fig. 5 Cross-sectional TEM images in W/Cu multilayered nanofilms after 6.4-MeV Xe^{23+} ions radiation: **a** W/Cu6, **b** W/Cu18, and **c** W/Cu24 to a fluence of 7.5×10^{14} ions·cm^{-2}; **d** W/Cu6, **e** W/Cu18, and **f** W/Cu24 to a fluence of 1.5×10^{15} ions·cm^{-2}. Reproduced with permission from Ref. [75]. Copyright 2017 Elsevier; **g** front view of Cu/W interfaces. The yellow and blue spheres represent Cu and W atoms, respectively, and the white spheres correspond to the He atoms located at the most stable sites. Reproduced with permission from Ref. [88]. Copyright 2016 Elsevier

to four competitive processes including ballistic effect, thermal spike effect, thermodynamic effect, and migration of defects and the absorption of interfaces. All of the experiments showed that the nanofilm with smaller period-thickness owns better resistance to particle irradiation. Based on energetic analysis [88], monovacancy-type and He impurity point defects at two different W/Cu semi-coherent interfaces and adjacent layers have been investigated. Figure 5g indicates the possible migration path for He atom in the Cu/W interface, and the point defects were greatly attracted by the W/Cu interface, especially the Cu vacancy at the interface. A strong influence of the relative orientation between the two metals existed in special interfaces. And these interfaces were candidates to build-up desired radiation-resistant multilayers due to its capability to restrain He bubbles.

3.3 Nanofilm tungsten containing non-metal layers for radiation resistance

Metal/non-metal interface can also play a critical role in the formation of a strongly immiscible combination. The large mixing enthalpy between tungsten and non-metal can ensure the phase stability of tungsten/non-metal multilayered nanofilms at different thickness size ranges.

Wang et al. [78] prepared two W/ZrO_2 nanofilms with different thickness periods (7 nm W/14 nm ZrO_2 and 70 nm W/140 nm ZrO_2). As shown in Fig. 6a and c, the W/ZrO_2 (7/14 nm) multilayer interfaces remained sharp and no intermixing of the layers was found after the 4 MeV Au irradiation. But in the W/ZrO_2 (70/140 nm) multilayer as shown in Fig. 6b and d, the ZrO_2 layer was found to grow as polymorphs of tetragonal and monoclinic phases. Figure 6e shows relationship between the average grain size and radiation displacement damage. Although there is no other characterization, it exhibited that the W/ZrO_2 multilayers nanofilm (7/14 nm) owned greater resistance to grain growth under radiation.

Thermal conductivity is another research hotspot in multilayer system in radiation environment. In addition to defect damage, radiation has a profound impact on the thermal conductivity of the nanofilm structure. In the multilayer nanofilms structure, thermal conductivity will dramatically decrease because the phonon propagation is hindered via large number of interface. For example, the thermal conductivity of W/ZrO_2 multilayers system can be decreased to 1 W/mK compared to that of individual components [89]. Therefore, these nanofilm could be applied in thermal barrier coating.

On the contrary, some critical component in the reactor is supposed to own good thermal conductivity to ensure heat can be transferred in time. The intrinsic thermal conductivity of nanofilm is high, and the radiation-induced defects will further hinder heat transfer. But it is interesting that thermal transport can be tailored by interfaces due to scattering, reflection, and mean free path shortening of phonons at interfaces [90, 91]. Si et al. [77] introduced graphene into tungsten-based multilayer nanofilms. Figure 7a–f demonstrates the microstructure of multilayer nanofilms with different period before and after He irradiation. And Fig. 7g–i are the close-up images of irradiated interfaces. W15/G maintained sharp interface, but interface in W30/G and W40/G became jagged and indistinct. Significantly, all He bubble chains began from the interface of W/G and expanded along the irradiation direction. In the small-period sample as detailed in Fig. 7g, the lengths of the non-agglomerated He bubble chain were about 7 nm, while aggregated He bubble chains in the large-period sample were over 11 nm, and the width of chains depended on the layer thickness. The above results proved that W/graphene nano-multilayers with the least period own the best resistance to He irradiation. And the radiation hardening resistance of nano-multilayers W/G was much more than that of pure W film (Fig. 7j). Moreover, the special bilayer nanofilms showed a high interfacial thermal conductivity (about 84 $MW \cdot m^{-2} \cdot K^{-1}$), which was attributed to the excellent matching between graphene and tungsten layer. The author pointed out that the effective

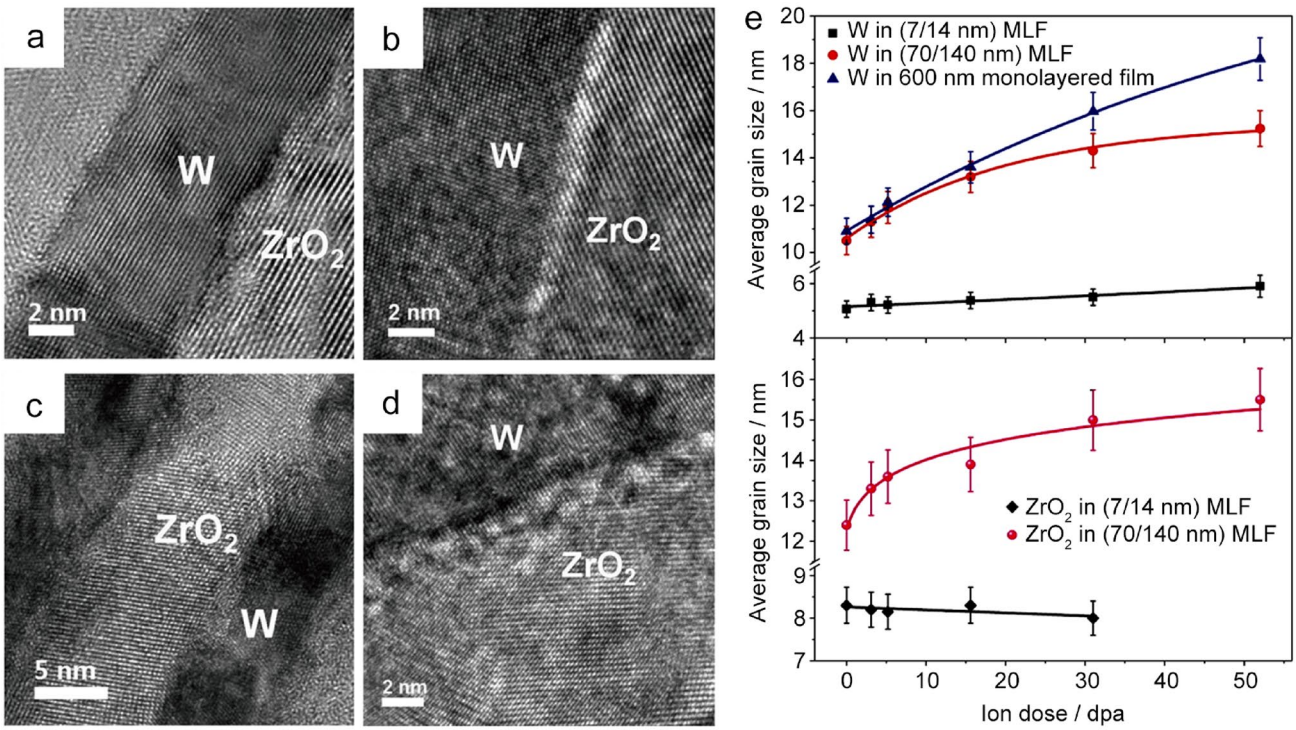

Fig. 6 HRTEM image of the W/ZrO_2 multilayer before irradiation: **a** W/ZrO_2 (7/14 nm) and **b** W/ZrO_2 (70/140 nm); W/ZrO_2 multilayer after 4 MeV irradiation (15.6 dpa): **c** W/ZrO_2 (7/14 nm) and **d** W/ZrO_2 (70/140 nm); **e** average grain size of W and ZrO_2 depending on displacement damage. Reproduced with permission from Ref. [78]. Copyright 2014 Elsevier

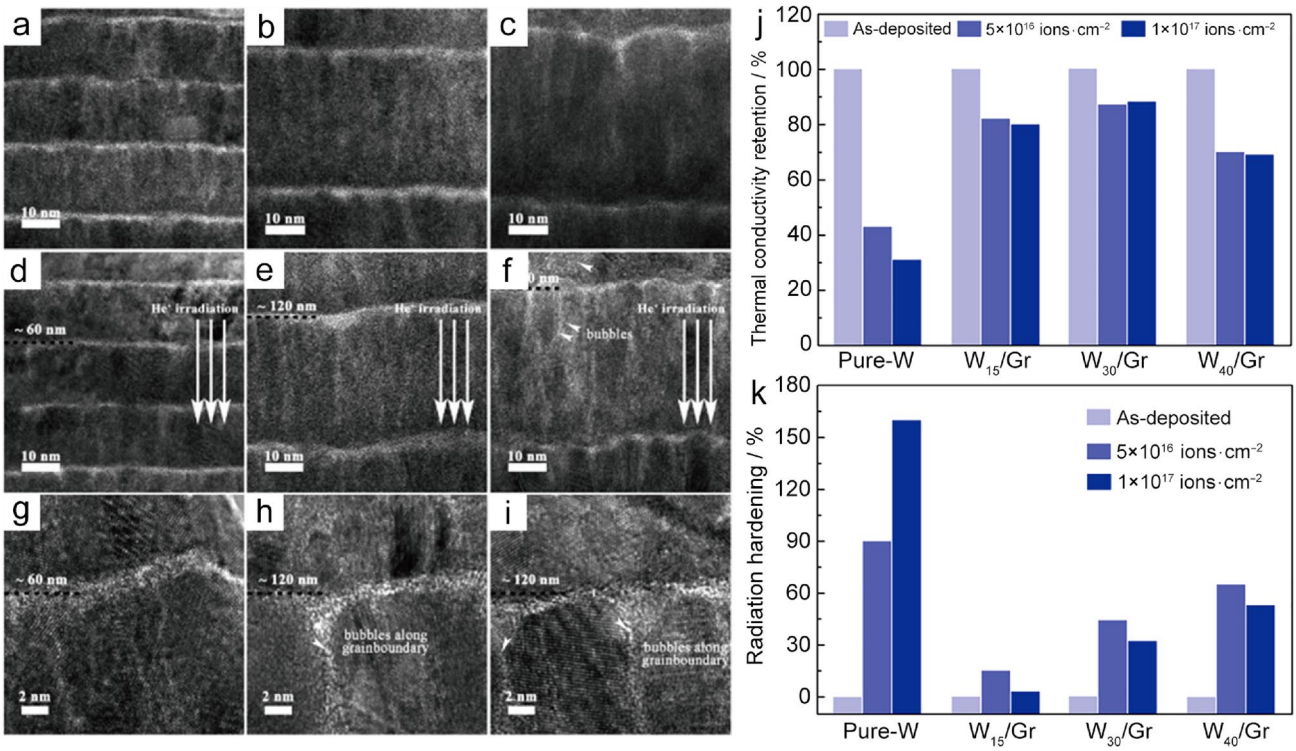

Fig. 7 TEM micrographs of as-deposited tungsten/graphene (W/G): **a** W15/G, **b** W30/G, and **c** W40/G; TEM micrographs of peak He concentration region irradiated by 50-keV He ion to a total influence of 5×10^{16} ions·cm^{-2}: **d** W15/G, **e** W30/G, and **f** W40/G; high magnification TEM micrographs of peak He concentration region: **g** W15/G, **h** W30/G, and **i** W40/G. Reproduced with permission from Ref. [77]. Copyright 2017 Wiley. **j** Radiation hardening, and **k** thermal conductivity retention of pure tungsten films and W/G multilayers with different periods after irradiation. Reproduced with permission from Ref. [92]. Copyright 2020 Elsevier

combination promoted the coupling of phonons and electrons in the process of heat transfer. As shown in Fig. 7k, the W15/G (W/graphene nanofilm with 15 nm W layer) showed an extremely high interfacial thermal conductivity retention (80%) after high-dose He radiation, while that of pure tungsten film was only 31% [92]. Thereby, W/C phase interfaces introduced by graphene intercalation in tungsten-based nanofilm structure have unexpected benefits to the interface thermal conductivity.

3.4 Outlook of nanofilm tungsten

All the above researches verified the remarkable improvement of radiation tolerance by constructing nanofilm W because of the introduction of large fraction interlayer interfaces. Nanofilm W has shown great potential in nuclear radiation protection, especially applied in the coating of PFMs.

However, complicated processes would be an obstacle in future applications. Up to now, W-based multilayer nanofilms are almost prepared by repeated magnetron sputtering or pulsed laser deposition, which are hard to process industrial size nanofilm at present. For instance, Fig. 8a illustrates the manufacture of W/graphene nanofilms. The multilayers are composed of repeatedly transferred graphene and deposited tungsten film, which is regarded to be complex and difficult to reproduce. Notably, the accumulative roll bonding (ARB) technology, as shown in Fig. 8b, has been applied in preparing Cu/Nb nanolaminate bulk material [93]. The lamellar composite was processed by repeatedly inserting fresh Nb layers during the modified ARB process, and the multilayer was improved in long-term mechanical integrity and resistance to He clusters damage. On the other hand, He et al. [94] proposed the W/reduced graphene oxide (RGO) bulk composite material with nacre-like architecture synthesized by spark plasma sintering as shown in Fig. 8c, which exhibited satisfied radiation hardening resistance. In spite of the thickness of each layer in micron, the researches provided inspiration to fabricate nanofilm W for bulk materials in the future.

Another challenge for nanofilm W that requires further understanding and resolution is lack of irradiation tests such as neutron and heavy ion at high energy. The irradiation researches of nanofilm W are almost based on the light ion to study the blister behavior and origin of radiation damage. Some efforts are put forward to discuss high dpa damage caused by swift heavy ions [75, 95], but systematically

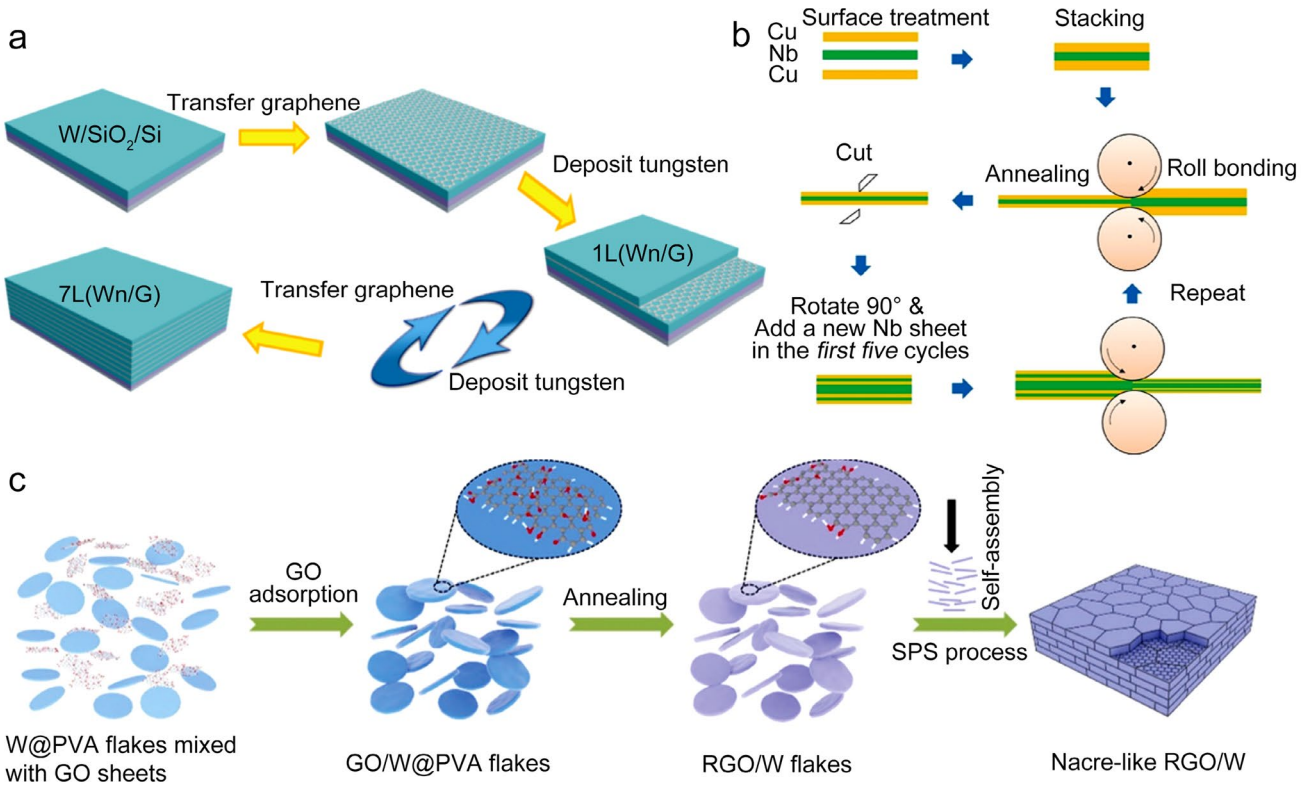

Fig. 8 Schematic diagram of preparation process of **a** W/G by repeated graphene transformation and tungsten deposition. Reproduced with permission from Ref. [77]. Copyright 2017 Wiley; **b** Cu/Nb nanolaminate by ARB. Reproduced with permission from Ref. [93]. Copyright 2020 Elsevier; **c** nacre-like W/RGO composites by SPS. Reproduced with permission from Ref. [94]. Copyright 2020 Elsevier

evaluating the application potential of nanofilm structure is hard with no more relevant radiation date.

4 Nanoporous tungsten for radiation resistance

Nanoporous material, a kind of three-dimensional open structure material, is widely applied in catalysis, energy, and structural materials [96–98] due to its high surface-to-volume ratio. As an interconnected network of ligaments, the nanoporous structure has been expected to be applied in radiation tolerance [99]. Free surfaces are considered to be perfect sinks for radiation defects, which are different from solid–solid interfaces in two nanostructures reviewed above. In the nanoporous structure, radiation damage cannot accumulate because the high density of free surfaces as sites for release of defects in excess of critical dose. Tungsten is suitable for the preparation of nanoporous metal. With both outstanding thermal stability and beneficial characteristic of nanoporous materials, the open-cell porous tungsten is the candidate material for the application in shielding against particle radiation.

4.1 Free surfaces and ligament size

Preliminary theoretical researches about radiation effect on the free surface of nanoporous structure have been explored. Typical metallic nanofoam is an important model to study the radiation behaviors of surfaces. In the Au nanofoam, the migration energies of point defects decreased, resulting in point defects continuously diffusing towards free surface, which retards the formation and growth of defect clusters around the free surfaces [100]. A series of studies [101–103] reported the radiation response of nanoporous Au in the experiments. Stacking fault tetrahedra (SFT) was found in Au ligaments after Ne irradiation, and the fault has been attributed to the vacancy collapse. Meanwhile, the interstitials annihilate at free surfaces leaving no damage, which can effectively reduce the radiation damage crisis caused by the retention of gas atoms in the interface.

The ligaments are the skeleton of nanoporous materials, and the ligament size was supposed to be appropriate to ensure the defect damage self-healing [104]. Overlarge ligament causes defects spreading to the surface which is slower than the cascade collision, but too small nano-ligament might melt or break during radiation. Hence, two ligament

size thresholds related to irradiation dose determine the radiation resistance of nanoporous materials. Farkas et al. [102] verified the comment by atomistic simulation that obvious size effect exists in nanoporous materials which is similar to nanocrystalline and nanofilm materials. Nanoporous Au possessed the best mechanical and radiation performance when the ligament size decreased to 1–10 nm, but undersized nano-pores gradually shrank and even disappeared with the increase of radiation dose [105, 106]. Experiments and calculation synergistically proved that a window exists in the parameter space where the nanoporous structure is remarkably radiation-tolerant due to its high density of free surfaces. Therefore, it is vital for the radiation-tolerant nanoporous material to artificially control the ligament size.

4.2 Status of nanofoam tungsten for radiation tolerance

The above work focused on the precious metal nanoporous materials, which is still far away from the engineering application in the reactor. It is of great significance for the research of nanoporous tungsten due to potential performance in harsh radiation environment.

Nanofoam tungsten is one of the earliest porous materials studied. The common method to obtain tungsten foam is to selectively dissolve the second-phase metal in tungsten alloy via chemical or electrochemical dealloying. And the soft and malleable phase would be completely dissolved first in the process of dissolution. W–Cu composites were an attempt to be etched with chloride ion to prepare open-cell nanoporous W with low strength of ligament [107]. These nanofoams would deform under indentation test due to formation of cracks and ligament collapse. Recently, a kind of ultra-strong tungsten nanofoam was tailored by reverse phase dissolution, to satisfy the need for desired mechanical properties in the radiation environment [108]. In this research, the nanoporous W contained nanoscale pore and distinct nanocrystalline architecture, as shown in Fig. 9a. Nano-grains around pore were connected by low-defective GBs, exhibiting yield strength beyond 2 GPa by nanoindentation test. Although there was lack of radiation data, these created nanoporous W is expected to own great radiation performance. W nanoparticles have been studied as a model system of nanofoam W for in situ TEM during He ion irradiation experiments [109]. And this system can be equivalent to the individual ligament without the influence of surrounding ligament. As

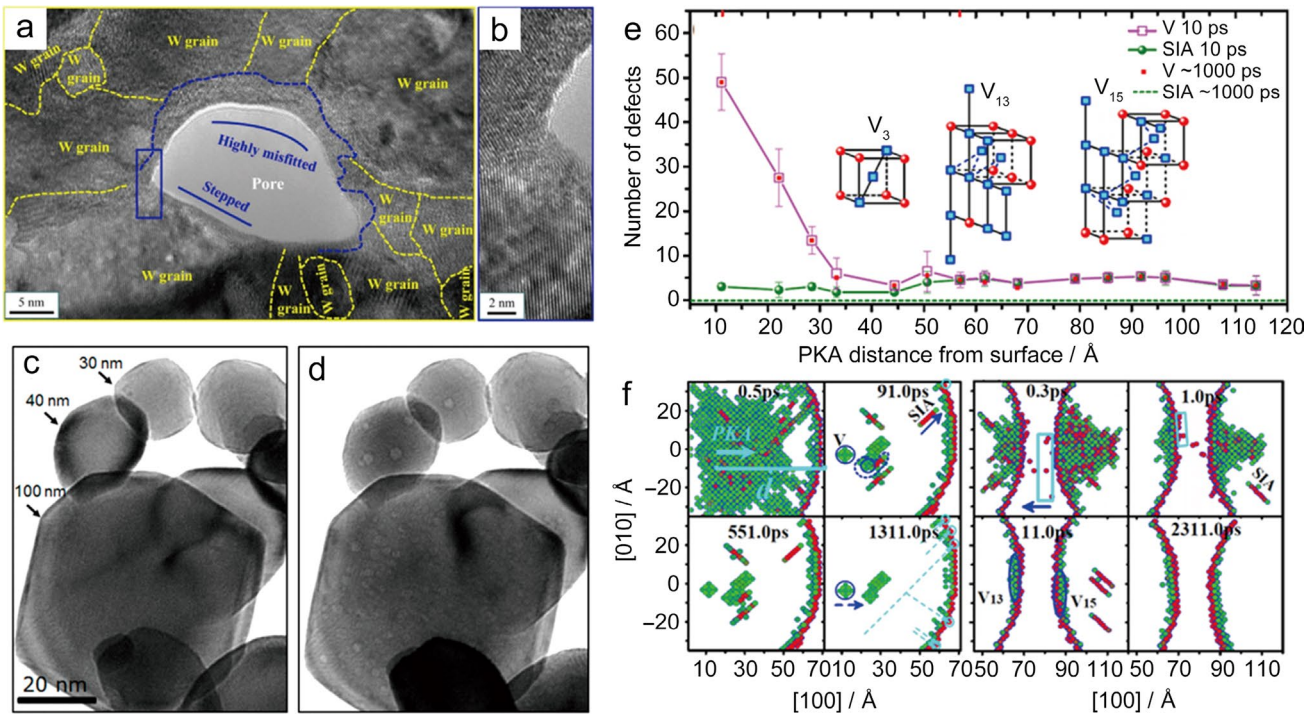

Fig. 9 **a** High-resolution TEM micrograph of nanoporous W exhibiting several nano-grains of tungsten around a nanopore. Nano-GBs are marked by yellow dashed lines. And a highly misfitted area along the free surface is indicated by a blue dashed line. **b** Magnified high-resolution TEM micrograph of the blue region area in **a**. Reproduced with permission from [108] Copyright 2020 Elsevier; Under-focus bright field-TEM images for W nanoparticles: **c** before radiation and **d** after radiation to a fluence of 1.1×10^{17} ions·cm^{-2} showing the bubble distributions in W nanoparticles of different sizes. Reproduced with permission from Ref. [109] Copyright 2018 MDPI; **e** variation of the defect number with the initial PKA distance from the surface; **f** representative snapshots of the collision cascades at positions B and A in **e**, respectively. Reproduced with permission from Ref. [110]. Copyright 2018 Elsevier

shown in Fig. 9c-d, a higher density of bubbles was found in 100 nm nanoparticles than that in 30 nm nanoparticles after He irradiation (1.1×10^{17} ions·cm^{-2}).

Under different scales simulation, Duan et al. [110] discussed the interaction of point defect with the surface of nanopore in W as shown in Fig. 9e, f. The annihilation of self-interstitial atom-vacancies occurs through the coupling of vacancies segregation from the matrix to the surface and the two-dimensional diffusion of self-interstitial atoms on the surface at 1000 K. The high density of surfaces is helpful to inhibit hydrogen retention and He bubble nucleation in nanoporous W, and thereby free surfaces are regarded to heal radiation damage better than grain boundaries. Wei et al. [111] studied the evolution of He bubbles on the surface of W under neutron irradiation utilizing molecular dynamics simulation. Different from non-irradiation conditions, more surviving vacancies and sputtered atoms formed under neutron radiation. And the bubbles are more likely to burst from the surface, especially from surfaces with low crystal face density. The vacancies and self-interstitial atoms were clustered on low index surface which was attributed to cluster absorption of these surfaces with previous defect clusters [112]. Eventually, the free surface became the locally concave–convex structure with radiation defects accumulation.

4.3 Nanochannel tungsten enhances radiation tolerance

Nanochannel W is a special nanoporous structure with a large number of channels caused by the gap between tungsten crystal columns, which seems to be more controllable for radiation application. This special porous structure was tailored via magnetron sputtering. And the channel size can be adjusted by controlling sputtering temperature and energy. Qin et al. [113] prepared nanochannel W films with different densities of free-pore. Figure 10a–d exhibits the section TEM image of nanochannels after He irradiation with commercial bulk tungsten as reference. The obvious

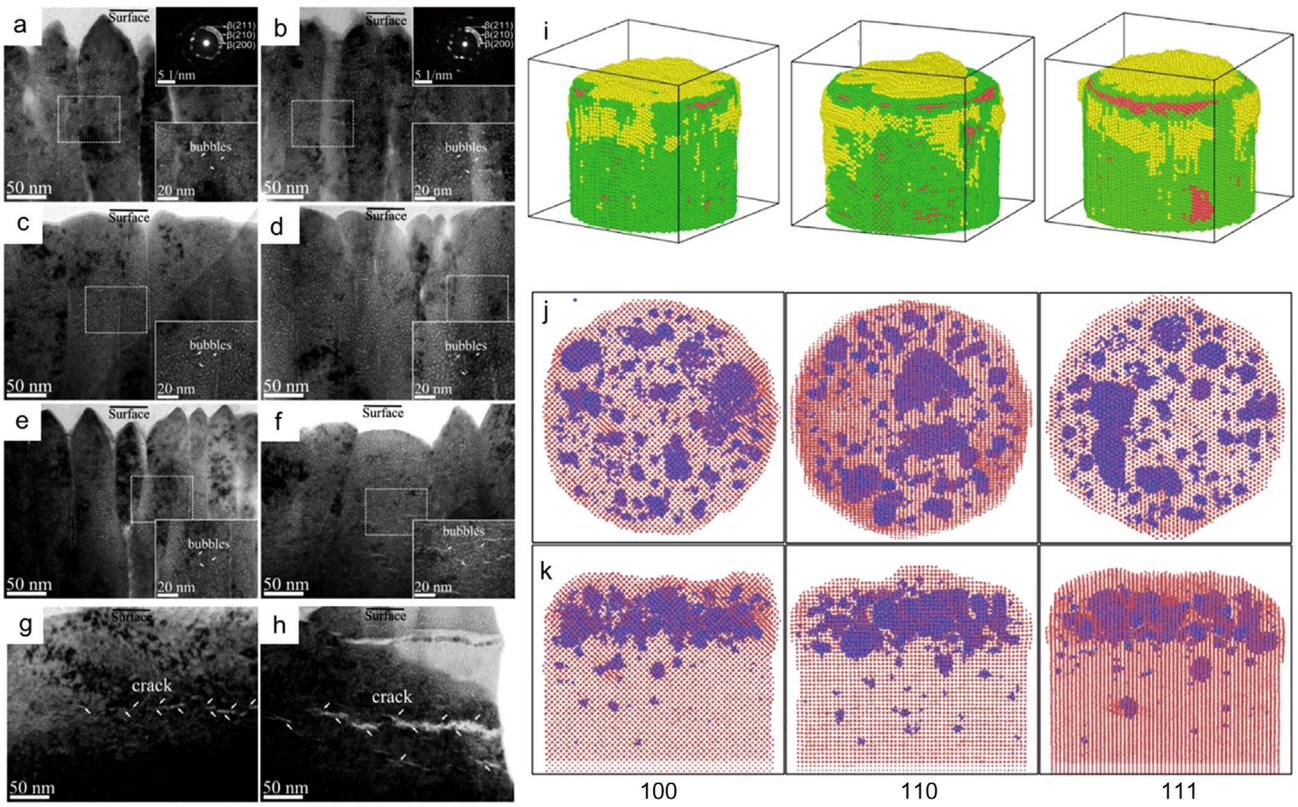

Fig. 10 TEM micrograph of the nanochannel W films and bulk W after radiation to the fluence of **a, c, e, g** 5×10^{17} and **b, d, f, h** 1×10^{18} ions·cm^{-2}. The tungsten films are prepared by various temperature and energy with **a, b** RT–150 W, **c**, **d** W–600–150 W, **e**, **f** W–600–50 W, and **g**, **h** pure W. The corresponding magnified images of the regions near 108 nm are marked by a dotted line. Reproduced with permission from Ref. [113]. Copyright 2018 Elsevier. **i** Simulated W columns (radius 6.34 nm) with three different orientations of {100}, {110}, and {111}, respectively, at 1500 K under He radiation to a fluence of 3.15×10^{16} ions·cm^{-2} by molecular dynamics. The light red, green, and yellow balls represent the inner W atoms, surface W atoms, and W adatoms. **j** Top and **k** side views of the helium atoms distribution in W columns (radius 6.34 nm) whose top surfaces are {100}, {110}, and {111}-oriented at 1500 K. The light red and blue balls represent the W and He atoms. Reproduced with permission from Ref. [117]. Copyright 2020 Elsevier

radiation-induced cracks were found in bulk materials with the fluence of 5×10^{17} and 1×10^{18} ions·cm^{-2} as shown in Fig. 10g, h, while no crack was found in tailored nanochannels W in the same context. Only He bubble chain appeared under higher dose irradiation, of which the size was much smaller than that of bulk W. According to the microstructure image, the transmuted He atom preferred to be released from nanochannels, rather than clustering into He bubbles in columnar crystal. In further works [114], 800 keV Kr^{2+} ion as pre-radiation was applied to simulate neutron irradiation and to probe the impact of displacement cascade damage on the behavior of transmutation gas. Unexpectedly, vacancies induced by Kr^{2+} irradiation improve the transmuted atoms trapping and suppress the aggregation of He bubbles and clusters. Meanwhile, the nanochannel structure can effectively suppress the formation of radiation-induced fuzz. Under the irradiation of high temperature and high beam He plasma at more than 5000 s, only tungsten in the range of 72 nm from top surface is transformed into fuzz structure in nanochannel thin films, while the surface of irradiated bulk tungsten alloy would be seriously eroded. The result indicated the effectively relieve thermal stress and maintain resistance to the He nucleation and "fuzz" formation behavior of nanochannel structure under high-temperature irradiation [115, 116].

The previous work [112] has shown that {100} surface in tungsten might own better resistance to morphology change due to the larger binding energy. Figure 10i–k shows MD simulation results [117] of three W columns with diverse orientation. Significantly, the columns with {100} top surface orientation have enhanced capability to release more He atoms than columns of other orientations after high He fluence exposure, indicating that nanochannel W can be prepared according to specific orientation to enhance the capacity of releasing He atoms and delaying the fuzz structure.

4.4 Challenge for nanoporous tungsten

Nanoporous W might be one of the most promising candidates for PFM due to its excellent resistance to the swelling caused by irradiated transmutation elements. Nanofoam and nanochannels structure reviewed above are nanoporous structure materials in the tolerant radiation field. However, several problems need to be overcome for the two kinds of porous structures before their further application:

Stable nanoporous structure is important to the application of radiation. The size and uniformity of nanopore affect the damage distribution of nanofoam W, but the pores are generally obtained by chemical or electrochemical etching of tungsten alloy. On the other hand, tungsten columnar crystals in nanochannel structure are considered to be metastable at high temperature, of which performance at elevated temperature needs to be further explored. The irradiation effect on the surface of tungsten shows obvious orientation correlation. Low index surface, especially surface {100}, own higher tolerance to irradiation damage, and better resistance to the morphology change than other surface. Thus, the orientation of grains should be taken into account in constructing nanoporous tungsten.

5 Summary and outlook

Nanostructured tungsten has attracted much attention due to its abundant grain boundaries, phase boundaries, and free surfaces, which is crucial in trapping defects, self-healing damage, or inhibiting the formation of "fuzz" structure when nanostructured tungsten is exposed to high-dose particles irradiation. There is a large amount of experimental evidence that the defect density in nanostructured tungsten is significantly reduced, and a variety of calculation and simulation tools assist in the study of how interface interacts with defects. Seemingly, no panacea has been found because each of nanostructure has known or potential drawbacks. But impressive radiation tolerance and other valuable characteristics determine the application prospect of nanostructured tungsten in future nuclear reactors. Several creative designs such as nanocrystalline, nanofilm, and nanoporous for the development of nanostructured tungsten exist that could dramatically improve the radiation resistance, though the mechanism of enhancing radiation resistance in three kinds of nanostructures is different.

Despite some exciting research in nanostructured tungsten for radiation resistance have been carried out, several problems remain to be solved. First of all, more irradiation experimental data are needed to evaluate the irradiation response of nanostructured tungsten to ensure these novel structural materials could work in their life span under harsh irradiation. Second, few studies have reported the reliability of nanostructures under the synergistic impact of high temperature and irradiation. In the high-temperature environment of the fusion reactor, it is still suspected whether the nanostructures would fail during the service life. Finally, the difficulty of large-scale fabrication of nanostructured tungsten has always hindered the practical application. Some alternative ideas could be referenced to inspire the preparation of bulk-grade nanostructured tungsten with the innovation of manufacturing technology. In the future, based on overcoming the above problems, nanostructured tungsten is expected to bring new creativity and vitality in practical radiation resistance application.

Acknowledgements This work was financially supported by the National Natural Science Foundation of China (Grant Nos. U1867215, 11875211, U1932134, 12074293 and 12025503), Hubei Provincial Natural Science Foundation (Grant No. 2019CFA036), and the

Fundamental Research Funds for the Central Universities (Grant No. 2042020kf0211).

References

1. Bolt H, Barabash V, Krauss W, Linke J, Neu R, Suzuki S, Yoshida N, Asdex Upgrade Team. Materials for the plasma-facing components of fusion reactors. J Nucl Mater. 2004;329–333:66.
2. Arshad K, Ding D, Wang J, Yuan Y, Wang Z, Zhang Y, Zhou ZJ, Liu X, Lu GH. Surface cracking of tungsten-vanadium alloys under transient heat loads. Nucl Mater Energy. 2015;3–4:32.
3. Tang Y, Qiu W, Chen L, Yang X, Song Y, Tang J. Preparation of W-V functionally gradient material by spark plasma sintering. Nucl Eng Technol. 2020;52:1706.
4. Wang Z, Yuan Y, Arshad K, Wang J, Zhou Z, Tang J, Lu GH. Effects of tantalum concentration on the microstructures and mechanical properties of tungsten-tantalum alloys. Fusion Eng Des. 2017;125:496.
5. Yang XL, Chen LQ, Qiu WB, Song YYP, Tang Y, Cui XD, Liu CS, Jiang Y, Zhang T, Tang J. Irradiation hardening behaviors of tungsten–potassium alloy studied by accelerated 3-MeV W^{2+} ions. Chinese Phys B. 2020;29(4):046102.
6. Yang X, Qiu W, Chen L, Tang J. Tungsten–potassium: a promising plasma-facing material. Tungsten. 2019;1(2):141.
7. Veleva L, Oksiuta Z, Vogt U, Baluc N. Sintering and characterization of W-Y and W–Y_2O_3 materials. Fusion Eng Des. 2009;84(7–11):1920.
8. Deng HW, Xie ZM, Wang YK, Liu R, Zhang T, Hao T, Wang XP, Fang QF, Liu CS. Mechanical properties and thermal stability of pure W and W–0.5 wt% ZrC alloy manufactured with the same technology. Mater Sci Eng A. 2018;715:117.
9. Xie ZM, Miao S, Zhang T, Liu R, Wang XP, Fang QF, Hao T, Zhuang Z, Liu CS, Lian YY, Liu X, Cai LH. Recrystallization behavior and thermal shock resistance of the W–1.0 wt% TaC alloy. J Nucl Mater. 2018;501:282.
10. Miao S, Xie ZM, Zhang T, Wang XP, Fang QF, Liu CS, Luo GN, Liu X, Lian YY. Mechanical properties and thermal stability of rolled W–0.5 wt% TiC alloys. Mater Sci Eng A. 2016;671:87.
11. Zinkle SJ, Busby JT. Structural materials for fission & fusion energy. Mater Today. 2009;12(11):12.
12. Knaster J, Moeslang A, Muroga T. Materials research for fusion. Nat Phys. 2016;12(5):424.
13. Ongena J, Koch R, Wolf R, Zohm H. Magnetic-confinement fusion. Nat Phys. 2016;12(5):398.
14. Nishijima D, Ye MY, Ohno N, Takamura S. Incident ion energy dependence of bubble formation on tungsten surface with low energy and high flux helium plasma irradiation. J Nucl Mater. 2003;313:97.
15. Ye MY. Effects of low energy and high flux Helium/Hydrogen plasma irradiation on tungsten as plasma facing material. Plasma Sci Technol. 2005;7(3):2828.
16. Kajita S, Takamura S, Ohno N, Nishijima D, Iwakiri H, Yoshida N. Sub-ms laser pulse irradiation on tungsten target damaged by exposure to helium plasma. Nucl Fusion. 2007;47(9):1358.
17. Baldwin MJ, Doerner RP. Formation of helium induced nanostructure "fuzz" on various tungsten grades. J Nucl Mater. 2010;404(3):165.
18. Wright GM, Brunner D, Baldwin MJ, Doerner RP, Labombard B, Lipschultz B, Lipschultz B, Terry JL, Whyte DG. Tungsten nano-tendril growth in the Alcator C-Mod divertor. Nucl Fusion. 2012;52(4):353.
19. Wright GM, Brunner D, Baldwin MJ, Bystrov K, Doerner RP, Labombard B, Lipschultz B, De Temmerman G, Terry JL, Whyte DG, Woller KB. Comparison of tungsten nano-tendrils grown in Alcator C-Mod and linear plasma devices. J Nucl Mater. 2013;438:S84.
20. Tanno T, Fukuda M, Nogami S, Hasegawa A. Microstructure development in neutron irradiated tungsten alloys. Mater Trans. 2011;52(7):1447.
21. Miyamoto M, Mikami S, Nagashima H, Iijima N, Nishijima D, Doerner RP, Yoshida N, Watanabe H, Ueda Y, Sagara A. Systematic investigation of the formation behavior of helium bubbles in tungsten. J Nucl Mater. 2015;463:333.
22. Ovid'ko IA, Sheinerman AG. Irradiation-induced amorphization processes in nanocrystalline solids. Appl Phys A. 2005;81(5):1083.
23. Pérez-Pérez FJ, Smith R. Structural changes at grain boundaries in bcc iron induced by atomic collisions. Nucl Instrum Meth B. 2000;164–165:487.
24. Chimi Y, Iwase A, Ishikawa N, Kobiyama M, Inami T, Okuda S. Accumulation and recovery of defects in ion-irradiated nanocrystalline gold. J Nucl Mater. 2001;297(3):355.
25. Samaras M, Derlet PM, Van Swygenhoven H, Victoria M. Radiation damage near grain boundaries. Philos Mag. 2003;83(31–34):3599.
26. Singh BN, Foreman AJE. Calculated grain size-dependent vacancy supersaturation and its effect on void formation. Philos Mag. 2006;29(4):847.
27. Demkowicz MJ, Hoagland RG, Hirth JP. Interface structure and radiation damage resistance in Cu-Nb multilayer nanocomposites. Phys Rev Lett. 2008;100(13):136102.
28. Zhang X, Hattar K, Chen Y, Shao L, Li J, Sun C, Yu K, Li N, Taheri ML, Wang H, Wang J, Nastasi M. Radiation damage in nanostructured materials. Prog Mater Sci. 2018;96:217.
29. Shen TD, Feng S, Tang M, Valdez JA, Wang Y, Sickafus KE. Enhanced radiation tolerance in nanocrystalline $MgGa_2O_4$. Appl Phys Lett. 2007;90(26):263115.
30. Sun C, Yu KY, Lee JH, Liu Y, Wang H, Shao L, Maloy SA, Hartwig KT, Zhang X. Enhanced radiation tolerance of ultrafine grained Fe–Cr–Ni alloy. J Nucl Mater. 2012;420(1–3):235.
31. Du C, Jin S, Fang Y, Li J, Hu S, Yang T, Zhang Y, Huang J, Sha G, Wang Y, Shang Z, Zhang X, Sun B, Xin S, Shen T. Ultrastrong nanocrystalline steel with exceptional thermal stability and radiation tolerance. Nat Commun. 2018;9(1):5389.
32. Ackland G. Controlling radiation damage. Science. 2010;327(5973):1587.
33. Wurster S, Pippan R. Nanostructured metals under irradiation. Scripta Mater. 2009;60(12):1083.
34. Zinkle SJ, Snead LL. Designing radiation resistance in materials for fusion energy. Annu Rev Mater Sci. 2014;44(1):241.
35. Wu ZM, Zhang J, Zhang J, Huang JC, Fan Y, Yu XH, Zhao YB, Zhu JL, Jin CQ, Wang P, Fu EG. Nanocrystalline W-based alloys with ultrahigh hardness and exceptional irradiation tolerance. Nucl Fusion. 2019;59(10):106050.
36. Faleschini M, Kreuzer H, Kiener D, Pippan R. Fracture toughness investigations of tungsten alloys and SPD tungsten alloys. J Nucl Mater. 2007;367–370:800.
37. Ameyama K, Oda E, Fujiwara H. Superplasticity and high temperature deformation behaviour in nano grain tungsten compacts. Materialwiss Werkst. 2008;39(4–5):336.
38. Efe M, El-Atwani O, Guo Y, Klenosky DR. Microstructure refinement of tungsten by surface deformation for irradiation damage resistance. Scripta Mater. 2014;70:31.
39. Wei Q, Jiao T, Ramesh K, Ma E, Kecskes L, Magness L, Dowding R, Kazykhanov V, Valiev R. Mechanical behavior and dynamic failure of high-strength ultrafine grained tungsten under uniaxial compression. Acta Mater. 2005;54:77.
40. Wei Q, Zhang H, Schuster B, Ramesh K, Valiev R, Kecskes L, Dowding R, Magness L, Cho K. Microstructure and mechanical

properties of super-strong nanocrystalline tungsten processed by high-pressure torsion. Acta Mater. 2006;54(15):4079.
41. El-Atwani O, Gonderman S, Efe M, De Temmerman G, Morgan T, Bystrov K, Klenosky D, Tian Q, Allain JP. Ultrafine tungsten as a plasma-facing component in fusion devices: effect of high flux, high fluence low energy helium irradiation. Nucl Fusion. 2014;54(8):083013.
42. Sun C, Song M, Yu KY, Chen Y, Kirk M, Li M, Wang H, Zhang X. In situ evidence of defect cluster absorption by grain boundaries in Kr ion irradiated nanocrystalline Ni. Metall Mater Trans A. 2013;44(4):1966.
43. Bai XM, Voter AF, Hoagland RG, Nastasi M, Uberuaga BP. Efficient annealing of radiation damage near grain boundaries via interstitial emission. Science 2010;327(5973):1631.
44. Liu LL, Tang Z, Xiao W, Wang Z. Self-healing mechanism of irradiation defects near Σ=11(113) grain boundary in copper. Mater Lett. 2013;109:221.
45. Chen D, Wang J, Chen T, Shao L. Defect annihilation at grain boundaries in alpha-Fe. Sci Rep. 2013;3:1450.
46. El-Atwani O, Hinks JA, Greaves G, Gonderman S, Qiu T, Efe M, Allain JP. In-situ TEM observation of the response of ultrafine- and nanocrystalline-grained tungsten to extreme irradiation environments. Sci Rep. 2014;4:4716.
47. El-Atwani O, Aydogan E, Esquivel E, Efe M, Wang YQ, Maloy SA. Detailed transmission electron microscopy study on the mechanism of dislocation loop rafting in tungsten. Acta Mater. 2018;147:277.
48. Wen M, Ghoniem NM, Singh BN. Dislocation decoration and raft formation in irradiated materials. Philos Mag. 2005;85(22):2561.
49. El-Atwani O, Esquivel E, Efe M, Aydogan E, Wang YQ, Martinez E, Maloy SA. Loop and void damage during heavy ion irradiation on nanocrystalline and coarse grained tungsten: Microstructure, effect of dpa rate, temperature, and grain size. Acta Mater. 2018;149:206.
50. El-Atwani O, Esquivel E, Aydogan E, Martinez E, Baldwin JK, Li M, Uberuaga BP, Maloy SA. Unprecedented irradiation resistance of nanocrystalline tungsten with equiaxed nanocrystalline grains to dislocation loop accumulation. Acta Mater. 2019;165:118.
51. Chen Z, Niu LL, Wang Z, Tian L, Kecskes L, Zhu K, Wei Q. A comparative study on the in situ helium irradiation behavior of tungsten: coarse grain vs nanocrystalline grain. Acta Mater. 2018;147:100.
52. Kong XS, Wu X, You YW, Liu CS, Fang QF, Chen JL, Luo GN, Wang Z. First-principles calculations of transition metal-solute interactions with point defects in tungsten. Acta Mater. 2014;66:172.
53. Tan XY, Li P, Luo LM, Xu Q, Tokunaga K, Zan X, Wu YC. Effect of second-phase particles on the properties of W-based materials under high-heat loading. Nucl Mater Energy. 2016;9:399.
54. Kurishita H, Amano Y, Kobayashi S, Nakai K, Arakawa H, Hiraoka Y, Takida T, Takebe K, Matsui H. Development of ultra-fine grained W-TiC and their mechanical properties for fusion applications. J Nucl Mater. 2007;367–370:1453.
55. Kurishita H, Kobayashi S, Nakai K, Arakawa H, Matsuo S, Takida T, Takebe K, Kawai M. Current status of ultra-fine grained W-TiC development for use in irradiation environments. Phys Scripta. 2007;T128:76.
56. Kurishita H, Kobayashi S, Nakai K, Ogawa T, Hasegawa A, Abe K, Arakawa H, Matsuo S, Takida T, Takebe K, Kawai M, Yoshida N. Development of ultra-fine grained W–(0.25–0.8) wt%TiC and its superior resistance to neutron and 3 MeV He-ion irradiations. J Nucl Mater. 2008;377(1):34.
57. El-Atwani O, Cunningham WS, Esquivel E, Li M, Trelewicz JR, Uberuaga BP, Maloy SA. In-situ irradiation tolerance investigation of high strength ultrafine tungsten-titanium carbide alloy. Acta Mater. 2019;164:547.
58. Fukuda M, Hasegawa A, Tanno T, Nogami S, Kurishita H. Property change of advanced tungsten alloys due to neutron irradiation. J Nucl Mater. 2013;442(1–3):S273.
59. Kurishita H, Matsuso S, Arakawa H, Hirai T, Linke J, Kawai M, Yoshida N. Development of nanostructured W and Mo materials. Adv Mater Res. 2008;59:18.
60. El-Atwani O, Li N, Li M, Devaraj A, Baldwin JKS, Schneider MM, Sobieraj D, Wrobel JS, Nguyen-Manh D, Maloy SA, Martinez E. Outstanding radiation resistance of tungsten-based high-entropy alloys. Sci Adv. 2019;5(3):eaav2002.
61. Li X, Zhang L, Dong Y, Gao R, Qin M, Qu X, Li J. Pressureless two-step sintering of ultrafine-grained tungsten. Acta Mater. 2020;186:116.
62. Dong Y, Yang H, Zhang L, Li X, Ding D, Wang X, Li J, Li J, Chen IW. Ultra-uniform nanocrystalline materials via two-step sintering. Adv Funct Mater. 2020;31(1):2007750.
63. Hu XX, Parish CM, Wang K, Koyanagi T, Eftink BP, Katoh Y. Transmutation-induced precipitation in tungsten irradiated with a mixed energy neutron spectrum. Acta Mater. 2019;165:51.
64. Zhang T, Xie Z, Yang J, Hao T, Liu C. The thermal stability of dispersion-strengthened tungsten as plasma-facing materials: a short review. Tungsten. 2019;1(3):187.
65. Monclús MA, Karlik M, Callisti M, Frutos E, Llorca J, Polcar T, Molina-Aldareguía JM. Microstructure and mechanical properties of physical vapor deposited Cu/W nanoscale multilayers: Influence of layer thickness and temperature. Thin Solid Films. 2014;571:275.
66. Xu J, Kamiko M, Zhou Y, Lu G, Yamamoto R, Yu L, Kojima I. Structure transformations and superhardness effects in V/Ti nanostructured multilayers. Appl Phys Lett. 2002;81(7):1189.
67. Wen S, Zong R, Zeng F, Gao Y, Pan F. Evaluating modulus and hardness enhancement in evaporated Cu/W multilayers. Acta Mater. 2007;55(1):345.
68. Tsoi M, Jansen AG, Bass J, Chiang WC, Tsoi VV, Wyder P. Generation and detection of phase-coherent current-driven magnons in magnetic multilayers. Nature. 2000;406(6791):46.
69. Gu C, Lian J, Li G, Niu L, Jiang Z. High corrosion-resistant Ni–P/Ni/Ni–P multilayer coatings on steel. Surf Coat Technol. 2005;197(1):61.
70. Costescu RM, Cahill DG, Fabreguette FH, Sechrist ZA, George SM. Ultra-low thermal conductivity in W/Al_2O_3 nanolaminates. Science. 2004;303(5660):989.
71. Bauer P, Dufour C, Jaouen C, Marchal G, Pacaud J, Grilhé J, Jousset JC. High electronic excitations and ion beam mixing effects in high energy ion irradiated Fe/Si multilayers. J Appl Phys. 1997;81(1):116.
72. Lin Z, Zhigilei LV, Celli V. Electron-phonon coupling and electron heat capacity of metals under conditions of strong electron-phonon nonequilibrium. Phys Rev B. 2008;77(7):430.
73. Wang ZG, Dufour C, Paumier E, Toulemonde M. The S_e sensitivity of metals under swift-heavy-ion irradiation: a transient thermal process. J Phys-Condens Mat. 1994;6(34):6733.
74. Li N, Fu EG, Wang H, Carter JJ, Shao L, Maloy SA, Misra A, Zhang X. He ion irradiation damage in Fe/W nanolayer films. J Nucl Mater. 2009;389(2):233.
75. Dong L, Zhang H, Amekura H, Ren F, Chettah A, Hong M, Qin W, Tang J, Hu L, Wang H, Jiang C. Period-thickness dependent responses of Cu/W multilayered nanofilms to ions irradiation under different ion energies. J Nucl Mater. 2017;497:117.
76. Chen F, Tang X, Huang H, Liu J, Li H, Qiu Y, Chen D. Surface damage and mechanical properties degradation of Cr/W multilayer films irradiated by Xe^{20+}. Appl Surf Sci. 2015;357:1225.
77. Si S, Li W, Zhao X, Han M, Yue Y, Wu W, Guo S, Zhang X, Dai Z, Wang X, Xiao X, Jiang C. Significant radiation tolerance and

moderate reduction in thermal transport of a tungsten nanofilm by inserting monolayer graphene. Adv Mater. 2017;29(3):1604623.
78. Wang H, Gao Y, Fu E, Yang T, Xue J, Yan S, Chu PK, Wang Y. Irradiation effects on multilayered W/ZrO_2 film under 4 MeV Au ions. J Nucl Mater. 2014;455(1–3):86.
79. Jayakody S, Chaudhuri J, Jankowski AF. X-ray characterization of annealed Cu/Ni multilayers. J Mater Sci. 1997;32(10):2605.
80. Misra A, Hoagland RG, Kung H. Thermal stability of self-supported nanolayered Cu/Nb films. Philos Mag. 2004;84(10):1021.
81. Knoedler HL, Lucas GE, Levi CG. Morphological stability of copper-silver multilayer thin films at elevated temperatures. Metall Mater Trans A. 2003;34(5):1043.
82. Zhang X, Fu EG, Li N, Misra A, Wang YQ, Shao L, Wang H. Design of radiation tolerant nanostructured metallic multilayers. J Eng Mater Technol. 2012;134(4):041010.
83. Li N, Martin MS, Anderoglu O, Misra A, Shao L, Wang H, Zhang X. He ion irradiation damage in Al/Nb multilayers. J Appl Phys. 2009;105(12):123522.
84. Misra A, Demkowicz MJ, Zhang X, Hoagland RG. The radiation damage tolerance of ultra-high strength nanolayered composites. Jom. 2007;59(9):62.
85. Zhang X, Li N, Anderoglu O, Wang H, Swadener JG, Höchbauer T, Misra A, Hoagland RG. Nanostructured Cu/Nb multilayers subjected to helium ion-irradiation. Nucl Instrum Meth B. 2007;261(1–2):1129.
86. Gao Y, Yang T, Xue J, Yan S, Zhou S, Wang Y, Kwok Dixon TK, Chu PK, Zhang Y. Radiation tolerance of Cu/W multilayered nanocomposites. J Nucl Mater. 2011;413(1):11.
87. Callisti M, Karlik M, Polcar T. Bubbles formation in helium ion irradiated Cu/W multilayer nanocomposites: Effects on structure and mechanical properties. J Nucl Mater. 2016;473:18.
88. González C, Iglesias R. Energetic analysis of He and monovacancies in Cu/W metallic interfaces. Mater Design. 2016;91:171.
89. Döring F, Major A, Eberl C, Krebs H-U. Minimized thermal conductivity in highly stable thermal barrier W/ZrO_2 multilayers. Appl Phys A. 2016;122(10):872.
90. Vineis CJ, Shakouri A, Majumdar A, Kanatzidis MG. Nanostructured thermoelectrics: big efficiency gains from small features. Adv Mater. 2010;22(36):3970.
91. Döring F, Eberl C, Schlenkrich S, Schlenkrich F, Hoffmann S, Liese T, Krebs HU, Pisana S, Santos T, Schuhmann H, Seibt M, Mansurova M, Ulrichs H, Zbarsky V, Münzenberg M. Phonon localization in ultrathin layered structures. Appl Phys A. 2015;119(1):11.
92. Si S, Wang J, Li J, Li W, Cong H, Liu J, Tang J, Jiang C, Xia R, Xiao X. Enhancing resistance to radiation hardening and radiation thermal conductivity degradation by tungsten/graphene interface engineering. J Nucl Mater. 2020;539:152348.
93. Gao R, Jin M, Han F, Wang B, Wang X, Fang Q, Dong Y, Sun C, Shao L, Li M, Li J. Superconducting Cu/Nb nanolaminate by coded accumulative roll bonding and its helium damage characteristics. Acta Mater. 2020;197:212.
94. He L, Si S, Xu H, Tang C, Liu J, Dong S, Jiang C, Xiao X. Enhanced mechanical property and radiation resistance of reduced graphene oxide/tungsten composite with nacre-like architecture. Compos Struct. 2020;245:112361.
95. Bagchi S, Singh F, Avasthi DK, Lalla NP. Thickness dependent effect of swift heavy ion irradiation in W/Ni superlattice multilayers. J Phys D Appl Phys. 2009;42(14):145414.
96. Fujita T, Guan P, McKenna K, Lang X, Hirata A, Zhang L, Tokunaga T, Arai S, Yamamoto Y, Tanaka N, Ishikawa Y, Asao N, Yamamoto Y, Erlebacher J, Chen M. Atomic origins of the high catalytic activity of nanoporous gold. Nat Mater. 2012;11(9):775.
97. Sayle TX, Ngoepe PE, Sayle DC. Simulating mechanical deformation in nanomaterials with application for energy storage in nanoporous architectures. ACS Nano. 2009;3(10):3308.
98. Hassan A, Ali G, Park YJ, Hussain A, Cho SO. Formation of a self-organized nanoporous structure with open-top morphology on 304L austenitic stainless steel. Nanotechnology. 2020;31(31):315603.
99. Beyerlein IJ, Caro A, Demkowicz MJ, Mara NA, Misra A, Uberuaga BP. Radiation damage tolerant nanomaterials. Mater Today. 2013;16(11):443–9.
100. Zhang CG, Li YG, Zhou WH, Hu L, Zeng Z. Anti-radiation mechanisms in nanoporous gold studied via molecular dynamics simulations. J Nucl Mater. 2015;466:328.
101. Fu EG, Caro M, Zepeda-Ruiz LA, Wang YQ, Baldwin K, Bringa E, Nastasi M, Caro A. Surface effects on the radiation response of nanoporous Au foams. Appl Phys Lett. 2012;101(19):191607.
102. Farkas D, Caro A, Bringa E, Crowson D. Mechanical response of nanoporous gold. Acta Mater. 2013;61(9):3249.
103. Caro M, Mook WM, Fu EG, Wang YQ, Sheehan C, Martinez E, Baldwin JK, Caro A. Radiation induced effects on mechanical properties of nanoporous gold foams. Appl Phys Lett. 2014;104(23):233109.
104. Bringa EM, Monk JD, Caro A, Misra A, Zepeda-Ruiz L, Duchaineau M, Abraham F, Nastasi M, Picraux ST, Wang YQ, Farkas D. Are nanoporous materials radiation resistant? Nano Lett. 2012;12(7):3351.
105. Chen Y, Yu KY, Liu Y, Shao S, Wang H, Kirk MA, Wang J, Zhang X. Damage-tolerant nanotwinned metals with nanovoids under radiation environments. Nat Commun. 2015;6:7036.
106. Li J, Fan C, Ding J, Xue S, Chen Y, Li Q, Wang H, Zhang X. In situ heavy ion irradiation studies of nanopore shrinkage and enhanced radiation tolerance of nanoporous Au. Sci Rep. 2017;7:39484.
107. Zhao M, Pfeifenberger MJ, Kiener D. Open-cell tungsten nanofoams: chloride ion induced structure modification and mechanical behavior. Results in Phys. 2020;17:103062.
108. Zhao M, Issa I, Pfeifenberger MJ, Wurmshuber M, Kiener D. Tailoring ultra-strong nanocrystalline tungsten nanofoams by reverse phase dissolution. Acta Mater. 2020;182:215.
109. Aradi E, Lewis-Fell J, Harrison RW, Greaves G, Mir AH, Donnelly SE, Hinks JA. Enhanced Radiation Tolerance of Tungsten Nanoparticles to He Ion Irradiation. Nanomaterials Basel. 2018;8(12):1052.
110. Duan G, Li X, Sun J, Hao C, Xu Y, Zhang Y, Liu W, Liu CS. Surface-structure dependence of healing radiation-damage mechanism in nanoporous tungsten. J Nucl Mater. 2018;498:362.
111. Wei G, Ren F, Qin W, Hu W, Deng H, Jiang C. Evolution of helium bubbles below different tungsten surfaces under neutron irradiation and non-irradiation conditions. Comp Mater Sci. 2018;148:242.
112. Hao C, Li X, Zhang Y, Xu Y, Jiang Y, Liu CS, Fang QF, Wang X, Zhang T. Effect of the accumulated vacancies and interstitials on the tungsten surface on the surface's role as defect sinks. Nucl Instrum Meth B. 2018;436:51.
113. Qin W, Ren F, Doerner RP, Wei G, Lv Y, Chang S, Tang M, Deng H, Jiang C, Wang Y. Nanochannel structures in W enhance radiation tolerance. Acta Mater. 2018;153:147.
114. Qin W, Wang Y, Tang M, Ren F, Fu Q, Cai G, Dong L, Hu L, Wei G, Jiang C. Microstructure and hardness evolution of nanochannel W films irradiated by helium at high temperature. J Nucl Mater. 2018;502:132.
115. Qin W, Jin S, Cao X, Wang Y, Peres P, Choi SY, Jiang C, Ren F. Influence of nanochannel structure on helium-vacancy cluster evolution and helium retention. J Nucl Mater. 2019;527:151822.
116. Qin W, Ren F, Zhang J, Dong X, Feng Y, Wang H, Tang J, Cai G, Wang Y, Jiang C. Helium retention in krypton ion pre-irradiated nanochannel W film. Nucl Fusion. 2018;58(2):026021.

117. Wei G, Li J, Li Y, Deng H, Jiang C, Ren F. A better nanochannel tungsten film in releasing helium atoms. J Nucl Mater. 2020;532:152044.

Dr. Wen-Qing Li received his Ph.D. in 2016 from Wuhan University, China. After three years of postdoctoral work at Wuhan University, he has been an associate professor in the School of Physics, Wuhan University. His research focuses on ion beam modification of nanomaterials, especially on modulating the performance of field-effect transistor (FET) and resistive random access memory (RRAM) via ion beam.

Dr. Xiang-Heng Xiao obtained his B.S. in 2001 and Ph.D. in 2008 from Wuhan University. He is a professor in the School of Physics and Technology, Wuhan University. His research field mainly focuses on interaction of energetic ions with matter, energy conversion, ion-beam modification of nanoscale material, etc.